Constant-Beamwidth Beamforming With Nonuniform Concentric Ring Arrays

Avital Kleiman, Israel Cohen, *Fellow, IEEE*, and Baruch Berdugo

***Abstract*—Solutions for frequency-invariant beamforming with concentric circular arrays are used in many applications, including microphone arrays and audio communication. However, existing methods focus on the azimuth-beamwidth and consider uniformly spaced circular arrays. This paper presents an approach to designing a constant elevation-beamwidth beamformer for nonuniform concentric ring arrays. The suggested beamformer aims to maximize the array directivity factor while maintaining fixed beamwidth over a wide range of frequencies. The introduced methodology simultaneously selects the ring placements and designs the beamformer weights that achieve optimal performance. We present the problem constraints and cost function, resulting in a sparse beamformer design. In addition, a uniformly spaced beamformer is incorporated into the optimization cost function to attain improved performance. Time-domain implementation of the ideal beamformer is also presented in this work. Furthermore, in the proposed array configuration, all sensors on each ring share the same weight value. Thus, the computational complexity and the physical hardware required in a physical setup are significantly reduced. Experimental results demonstrate the advantages of the nonuniform beamformer compared to a uniform beamformer in terms of directivity index, white noise gain, and sidelobe attenuation.**

***Index Terms*—Array processing, concentric circular array, constant-beamwidth beamforming, microphone array, frequency-invariant beamforming, directivity-factor, white-noise-gain, sparse design.**

I. Introduction

APPLICATIONS of audio communication involve processing of broadband signals while suppressing interferences and noises [1]–[3]. Hence, many frequency invariant (FI) broadband beamformer designs are employed in these applications, providing enhanced performances in various tasks while avoiding distortion of the signal of interest [4]–[13]. Choosing the array geometry has a significant impact on the performance. Therefore, the array geometry should suit the problem specifications. In three-dimensional (3D) problems, the planar array geometry is preferred compared to the uniform linear array (ULA) geometry (which is widely used in numerous beamforming algorithms in the literature) [14]–[17]. Due to its symmetric geometry and the all-azimuth scan capability, the uniform circular array (UCA) geometry was the main focus of the planar array beamformer designs presented in the last decade. Uniform concentric circular arrays (UCCAs), constructed of multiple rings, exhibited superior performance in the direction of arrival (DOA) estimation, broadband beamforming, and noise suppression [18]–[22].

Maintaining a constant beamwidth over a wide range of frequencies is a significant challenge when designing a wideband beamformer. Conventional broadband beamformers (like delay-and-sum [1]) apply different spatial filters at different frequencies, which results in narrowing the mainlobe as the frequency increases. Thus, any change in the direction of the received signal distorts the beamformer output signal. To avoid signal distortion, several FI beamforming methods have been proposed for UCCAs over the last decade. A common criterion in designing an FI beampattern is the minimum mean-square error (MMSE). This approach was suggested in [23]–[25], minimizing the error between the attained beampattern and the desired beampattern. Following, a fixed broadband pattern was designed in [26], [27] by solving a second-order cone programming problem. Employing convex optimization to attain the desired beampattern on circular geometry was also presented in [28]–[31]. In addition, differential sensor UCCAs were investigated in [32]–[34]. While providing enhanced performance in terms of beampattern irregularities and steering flexibility, the suggested beamformers suffer from several disadvantages. First, most UCCA FI beamformers consider the scenario in which the signal of interest arrives from the horizontal plane. However, in practical 3D applications, the elevation angle is not restricted to 90°. The assumption of arbitrary elevation angle directly affects the directivity factor (DF) and the white-noise-gain (WNG), important performance measures of the array. Second, the beamformer design mostly focuses on minimizing the MMSE between the desired beampattern and the actual beampattern over a range of frequencies. Relaxing the restriction of the desired beampattern outside the mainlobe potentially provides superior performance in terms of beamwidth consistency, computational complexity, and the number of physical resources required in the setup [35]–[37]. Furthermore, the planar array beampattern characteristics can be utilized to efficiently implement the beamformer in the time domain, as presented in [38].

Several constant beamwidth beamformers were suggested in the literature for ULAs [39]–[42]. Recently, constant beamwidth beamformers for UCCAs were presented in [43], [44], enabling control of the elevation and azimuth beamwidth by weighting

Manuscript received November 23, 2021; revised April 7, 2022 and May 28, 2022; accepted May 29, 2022. Date of current version June 15, 2022. This work was supported by the Pazy Research Foundation. The associate editor coordinating the review of this manuscript and approving it for publication was Dr. Keisuke Kinoshita. *(Corresponding author: Avital Kleiman.)*

The authors are with the Andrew and Erna Viterbi Faculty of Electrical & Computer Engineering, Technion–Israel Institute of Technology, Haifa 3200003, Israel (e-mail: avital.kleiman@gmail.com; icohen@ee.technion.ac.il; bbaruch@technion.ac.il).

Digital Object Identifier 10.1109/TASLP.2022.3181419

the sensors on each ring. In addition, in [45] a window-based approach was employed on UCCA to attain fixed beamwidth. Both methods considered a uniformly-spaced ring array and preselected window shape of the beamformer weights.

This paper introduces constant beamwidth beamformers with improved DF, designed for UCCA geometry. The beamformers are diverse based on the degree of freedom in the design. First, we define a quadric programming optimization problem [46], aiming to maximize the DF while maintaining a constant beamwidth on a set of linearly spaced UCCA. Since the geometry is set, we perform the optimization on each frequency bin individually. Following this, we propose a constant beamwidth beamformer with no predefined radii locations. To achieve the maximal DF while maintaining the specified beamwidth, we propose a methodology to simultaneously choose the optimal ring locations and design the beamformer weights. The number of rings in the array is specified before performing the optimization. The optimal solution is chosen from a rigid grid of possible radii and performed coherently over all the frequency bins. To ensure equal or better DF compared to the incoherent beamformer, the DF of the incoherent beamformer is incorporated in the nonuniform beamformer cost function.

In the design process, we utilize concentric ring arrays (CRAs). In all of the suggested beamformers the microphones in each ring share joint weights. While eliminating beam steering ability, the proposed restrictions enable an analog summation of all the microphone signals on each ring before sampling, thus enabling a single A/D sampler per ring. Hence, in addition to simplifying the computational complexity of the design, the suggested beamformers require fewer resources in a physical setup.

The rest of this work is organized as follows: Section II presents the problem formulation, CRA design, and performance metrics. In Section III, we describe the optimization constraints, the cost function, and design methodologies. In Section IV, we evaluate the performance of the proposed beamformers. Finally, some conclusions are drawn in Section V.

II. Problem Formulation and Performance Measures

Consider a discrete CRA composed of M rings, containing N_m $(m = 1, 2, \ldots, M)$ microphones in each ring. We refer to the CRA as discrete since it is constructed of individual microphones rather than a continuous ring. The microphone elements are equally spaced, receiving a source signal (steered to broadside) in the farfield, as shown in Fig. 1.

Denoting the radius of the m^{th} ring as r_m, the placement of the k^{th} microphone ($k \in [1, N_m]$) on a Cartesian coordinate system can be expressed as

$$r_{m,k} = r_m \left(\cos\ \psi_{m,k}, \sin\ \psi_{m,k}, 0\right) , \tag{1}$$

where $\psi_{m,k}$ is the angular position of the k^{th} microphone on the m^{th} ring, measured anti-clockwise from the x-axis:

$$\psi_{m,k} = \frac{2\pi\,(k-1)}{N_m} . \tag{2}$$

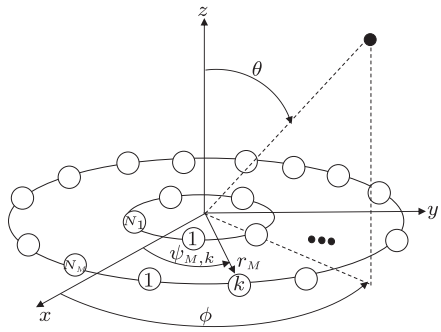

Fig. 1. Illustration of a CRA with M rings. $\psi_{m,k}$ indicates the angular position of the k^{th} element on the m^{th} ring, constructed of N_m elements. The elevation and azimuth angles are marked by θ, ϕ accordingly.

Considering a farfield broadband plane wave $x(t)$ impinging the CRA from direction (θ, ϕ), where ϕ is the azimuth angle and θ is the elevation angle, the signal arriving at any microphone can be represented as

$$y_{m,k}(t) = x\left(t - \tau_{m,k}\right) , \tag{3}$$

$$\tau_{m,k} = \frac{r_m \sin\theta \cos\left(\phi - \psi_{m,k}\right)}{\mathrm{c}} , \tag{4}$$

where c is the signal propagation speed, i.e., $340\frac{\mathrm{m}}{\mathrm{s}}$ for speech signals propagating in the air. When defining the problem in the frequency domain, the signal model is given by

$$Y_{m,k}(f) = \mathrm{e}^{-\mathrm{j}2\pi f \tau_{m,k}} X(f) , \tag{5}$$

where f is the temporal frequency and j is the imaginary unit with $\mathrm{j}^2 = -1$. Collecting all the data received across all the microphones of the m^{th} ring, we get

$$\begin{aligned} \underline{\boldsymbol{Y}}_m(f) &= \left[Y_{m,1}(f), Y_{m,2}(f), \ldots, Y_{m,N_m}(f)\right] \\ &= \underline{\boldsymbol{d}}_m\left(f, \theta, \phi\right) X(f) , \end{aligned} \tag{6}$$

where $\underline{\boldsymbol{d}}_m(f, \theta, \phi)$ is the steering vector of the m^{th} ring:

$$\underline{\boldsymbol{d}}_m\left(f, \theta, \phi\right) \triangleq \begin{bmatrix} \mathrm{e}^{\mathrm{j}\frac{2\pi r_m f}{\mathrm{c}}\cos(\phi - \psi_{m,1})\sin\theta} \\ \mathrm{e}^{\mathrm{j}\frac{2\pi r_m f}{\mathrm{c}}\cos(\phi - \psi_{m,2})\sin\theta} \\ \vdots \\ \mathrm{e}^{\mathrm{j}\frac{2\pi r_m f}{\mathrm{c}}\cos(\phi - \psi_{m,N_m})\sin\theta} \end{bmatrix} . \tag{7}$$

We can describe the CRA steering vector by concatenating the M rings steering vectors:

$$\underline{\boldsymbol{d}}\left(f, \theta, \phi\right) = \left[\underline{\boldsymbol{d}}_1^T\left(f, \theta, \phi\right), \ldots, \underline{\boldsymbol{d}}_M^T\left(f, \theta, \phi\right)\right]^T , \tag{8}$$

where ^{T} denotes the conjugate transpose operator.

This paper proposes a beamformer with constant elevation beamwidth and an improved DF. We propose that all microphones in a ring share one amplification in a given frequency f. The weight applied on the m^{th} ring is denoted by $H_m(f)$. A similar approach was taken in other 3-D array beamformers in the literature [29], [47], [48]. In practical applications, designing the beamformer with joint weights provides two advantages: first, sharing the same weight value across all microphones on each ring enables an analog summation of the output signals

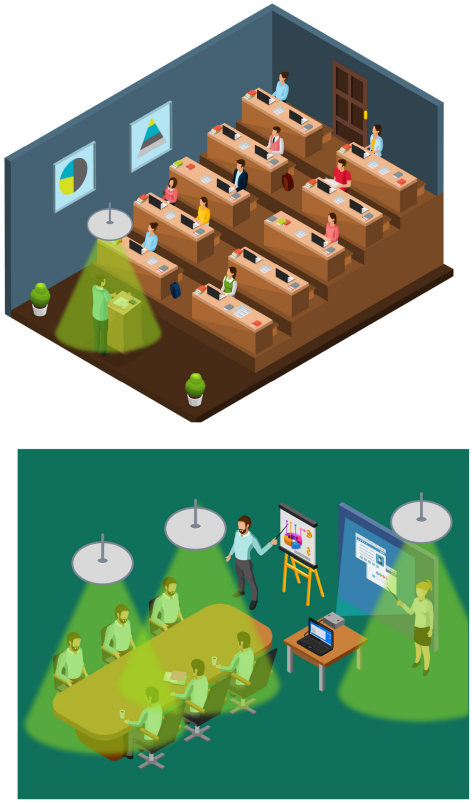

Fig. 2. Conference room and lecture hall illustration with circular ceiling array covering multiple beamforming zones.

before sampling. The array costs and maintenance would be lower with this design due to the reduced hardware requirements. Second, the number of variables to optimize is significantly lower, as it is determined by the number of rings in the array rather than the number of individual microphones. For this reason, both the optimization process and the computational complexity are lower. The suggested design can be incorporated as part of a ceiling sensors system, providing predefined coverage areas. Thus, by determining the required recording zones, one can eliminate the need for beam-steering. By designing a designated CRA beamformer with the desired beamwidth, the area of interest can be covered while significantly lowering the cost and complexity of the system. An illustration of the proposed ceiling array beamformer in multi-speaker settings like lecture halls and auditoriums is shown in Fig. 2. While the need for steering is unnecessary in the proposed system (so CRAs can be utilized), the beamformer design should support a pre-determined elevation beamwidth to cover the recording zone.

Under the joint weights design constraint, we define the weight vector applied to the m^{th} ring as:

$$\underline{\boldsymbol{h}}_m(f) = H_m(f)\underline{\mathbf{1}}_{1\times N_m}\,, \tag{9}$$

where $\underline{\mathbf{1}}_{1\times N_m}$ is the all-ones vector of length N_m. The total weight vector applied to the array at frequency f is achieved by concatenating all the rings weight vectors into a $(N\times 1)$ vector:

$$\underline{\boldsymbol{h}}(f) = \left[\underline{\boldsymbol{h}}_1(f),\ldots,\underline{\boldsymbol{h}}_M(f)\right]^T\,, \tag{10}$$

where N is the total number of microphones in the array $N \triangleq \sum_{m=1}^{M} N_m$. The summation of all the weighted output signals yields the CRA beampattern, i.e.,

$$\begin{aligned}\mathcal{B}\left[\underline{\boldsymbol{h}}(f),\theta,\phi\right] &= \underline{\boldsymbol{h}}^T(f)\underline{\boldsymbol{d}}\,(f,\theta,\phi)\\ &= \sum_{m=1}^{M} H_m(f)\sum_{k=1}^{N_m} \mathrm{e}^{\mathrm{j}\frac{2\pi r_m f}{\mathrm{c}}\cos(\phi-\psi_{m,k})\sin\theta}\,.\end{aligned} \tag{11}$$

A property of the discrete CRA array factor shows that with sufficient numbers of microphones on the rings, the beam pattern of the m^{th} ring is equivalent to a continuous ring of the same radius [47]. The continuous ring beampattern can be approximated by a zero-order Bessel function and is independent of the azimuth angle ϕ [49]. As a result, without loss of generality, one can choose $\phi \triangleq 0$, which yields

$$\mathcal{B}\left(\underline{\boldsymbol{h}}(f),\theta\right) = \sum_{m=1}^{M} H_m(f)N_m\mathcal{R}_m\left(f,\theta\right)\,, \tag{12}$$

where

$$\mathcal{R}_m\left(f,\theta\right) = \frac{1}{N_m}\sum_{k=1}^{N_m} \mathrm{e}^{j\frac{2\pi r_m f}{\mathrm{c}}\cos\psi_{m,k}\sin\theta} \tag{13}$$

denotes the discrete ring response. By examining the discrete ring response characteristics, we note that the beamwidth is narrower as the frequency increases. Hence, constant beamwidth can be maintained by weighting several ring responses with varying radii and weights as the frequency increases. The optimal selection of these components under specified constraints will be presented in the following.

Each ring in the CRA is constructed from equally spaced omnidirectional microphones. To avoid spatial aliasing the inter-sensor distance δ should be smaller than half the minimal wavelength λ_{min} [49], meaning that $\delta \le \lambda_{\text{min}}/2$. Consequently, the inner spacing on each ring should satisfy

$$\delta_m = 2r_m\sin\left(\frac{\pi}{N_m}\right) \approx \frac{2\pi r_m}{N_m} \le \frac{\mathrm{c}}{2f_m^{\max}}\,, \tag{14}$$

where δ_m denotes the inner spacing between two adjacent microphones on the m^{th} ring. The highest frequency in which the m^{th} ring is effective in the beamforming process is marked by $f_m^{\max}$. Thus, in frequencies in the range where $f_m^{\max} < f$ the m^{th} ring is completely attenuated. From (14), the number of equally spaced elements in ring m is given by

$$N_m = \left\lceil \frac{4\pi r_m f_m^{\max}}{\mathrm{c}} \right\rceil. \tag{15}$$

Since the number of microphones in each ring should be an integer, the value in (15) is rounded up.

The DF is an important characteristic of any beamformer [50]. Hence, one of the main goals of the proposed beamformers is to maximize the DF of the CRAs. The DF denotes the relative power between the beampattern in the direction-of-interest $(\theta_{\mathrm{d}},\phi_{\mathrm{d}})$ with respect to the entire 3-D beampattern. The DF can be interpreted as the beamformer's ability to suppress spatial

noise from directions other than the look direction. The DF can be written as [1]

$$\mathcal{D}(f) = \frac{\left|\mathcal{B}\left(f,\theta_{\mathrm{d}},\phi_{\mathrm{d}}\right)\right|^2}{\frac{1}{4\pi}\int_0^{\pi}\int_0^{2\pi}\left|\mathcal{B}\left(f,\theta,\phi\right)\right|^2\sin\theta d\phi d\theta} = \frac{\left|\underline{\boldsymbol{h}}^T(f)\underline{\boldsymbol{d}}\left(f,\theta_{\mathrm{d}},\phi_{\mathrm{d}}\right)\right|^2}{\underline{\boldsymbol{h}}^T(f)\Gamma(f)\underline{\boldsymbol{h}}(f)}, \tag{16}$$

where $\Gamma(f)$ is the pseudo-coherence matrix whose elements are

$$\Gamma_{i,j}(f) = \mathrm{sinc}\left(\frac{2\pi f\delta_{i,j}}{\mathrm{c}}\right), \tag{17}$$

where $\delta_{i,j}\ 1 \le i,j \le N$ is the Euclidean distance between two microphones, i and j, in the array. While the DF is an important measure of the beamformer performance (especially in 3-D broadband applications), most of the existing works on designing UCCA beamformers do not consider the DF as an optimization parameter. The beamforming algorithms include DF optimization in the following sections, and the results are presented in Section IV. For simplicity, all the results shown in this paper refer to the direction of interest as the boresight direction of the CRA.

Another performance measure is the white noise gain (WNG), which measures the array gain in a spatially uncorrelated noise environment. The WNG is an indicator of the beamformer robustness to microphones imperfections and is calculated by

$$\mathcal{W}(f) = \frac{\left|\underline{\boldsymbol{h}}^T(f)\underline{\boldsymbol{d}}\left(f,\theta_{\mathrm{d}},\phi_{\mathrm{d}}\right)\right|^2}{\underline{\boldsymbol{h}}^T(f)\underline{\boldsymbol{h}}(f)}. \tag{18}$$

III. Array Pattern Synthesis

In this section, a nonuniform constant beamwidth beamformer is suggested. The CRA has no pre-arranged ring locations selected dynamically in the design process. The beamformer weights are designed by solving a quadratic programming optimization problem. The objective of the optimization problem is to maximize the DF under a set of constraints to ensure constant beamwidth. The user-defined parameters are the desired beamwidth and the number of rings in the CRA. Ultimately, the sparse problem solution selects a set of ring locations out of a rigid grid of possible radii. Since the ring locations should be consistent for all frequencies, the optimization is performed over the entire frequency band. In this section, an additional beamformer is presented. This design is proposed for uniformly spaced CRAs, solving an equivalent optimization problem on a predefined set of rings. The result of the uniform beamformer approach is then used in the nonuniform beamformer to attain superior performance.

The following section describes several components in the beamformer design: First, the problem constraints are presented in Section III-A. The optimization constraints are defined as constant beamwidth over a wide band of frequencies while selecting a subset of rings out of a radii grid. Next, Section III-B discusses the optimization cost function. The cost function is constructed of a weighted summation of the DF over different frequencies. The frequencies are weighted based on the result of an additional optimization problem, designed for uniformly spaced CRA. Hence, we present the uniform CRA beamformer and the weighting method. The uniform beamformer performance will be shown in Section IV compared to the nonuniform beamformer. Finally, the time-domain implementation of the ideal beamformer is suggested in Section III-C.

We denote the uniformly discretized frequency space as $\{f_j\}_{j=1}^{J} \in \Omega$, containing J frequency bins. A set of ring positions is selected out of a high-resolution grid of possible ring positions by solving an optimization problem. The grid from which the ring locations are chosen is denoted by $\underline{\boldsymbol{r}} = [r_1, r_2, \ldots, r_{N_{\mathrm{R}}}]$. The grid vector contains N_{R} radii, indicating the number of optional ring radii in the grid. By setting the number of desired rings in the optimized array to M, the objective of the optimization problem is to find a set of M radii out of the possible N_{R} radii. Therefore, $\forall f_j\ \{f_j\}_{j=1}^{J} \in \Omega$ the weights vector applied on the array satisfies:

$$\underline{\boldsymbol{h}}\left(f_j\right) = \begin{cases} \{H_k\left(f_j\right)\}_{k\in\mathcal{K}}, & \text{for selected rings} \\ 0, & \text{otherwise,} \end{cases} \tag{19}$$

where $\mathcal{K}$ is the set of M chosen indices i.e. $\mathcal{K} \subseteq [1, N_{\mathrm{R}}]$. The chosen indices should be identical over the entire frequency space Ω.

A. Optimization Constraints

The beamformer is designed to have frequency-invariant characteristics by incorporating several constraints on the beampattern. First, to ensure that rings selected between different frequencies are all the same, a binary mask variable is introduced $\boldsymbol{\mathcal{M}}$. The binary mask is a matrix of size $N_{\mathrm{R}} \times J$. Each column of $\boldsymbol{\mathcal{M}}$, constructed of nulls and ones, indicates the selected radii at the corresponding frequency bin. Accordingly, given a grid of size $N_{\mathrm{R}} = 5$ and selected radii at 1, 3, and 5, the binary mask will be of the form:

$$\boldsymbol{\mathcal{M}}_{5\times J} = \begin{pmatrix} 1 & 1 & 1 & \cdots & 1 \\ 0 & 0 & 0 & \cdots & 0 \\ 1 & 1 & 1 & \cdots & 1 \\ 0 & 0 & 0 & \cdots & 0 \\ 1 & 1 & 1 & \cdots & 1 \end{pmatrix}. \tag{20}$$

Note that in order for the ring selection to be identical over the entire frequency range, the columns of $\boldsymbol{\mathcal{M}}$ should be identical. This dependency is achieved by introducing a constraint on the matrix columns, shown in (25). Similarly, we define the weight matrix applied on the array as $\boldsymbol{\mathcal{H}}$. The array weight matrix is constructed from the CRA weights vectors over the entire frequency range, as shown in (10):

$$\boldsymbol{\mathcal{H}} = \begin{bmatrix} \underline{\boldsymbol{h}}\left(f_1\right) & \underline{\boldsymbol{h}}\left(f_2\right) & \cdots & \underline{\boldsymbol{h}}\left(f_J\right) \end{bmatrix}. \tag{21}$$

The binary mask is used to enforce the selected radii on the beamformer weight matrix. The correlation is achieved by the following constraint:

$$\mathcal{C}_1 \ : \ \mathbf{0} \le \boldsymbol{\mathcal{H}} \le \boldsymbol{\mathcal{M}}, \tag{22}$$

where $\mathbf{0}$ is the zero matrix of size $N_{\mathrm{R}} \times J$. Constraint (22) compels the beamformer weights to be different from null only for the selected rings. That is, for each matrix element in indices (k, j) we get

$$\boldsymbol{\mathcal{H}}_{(k,j)} = \begin{cases} H_k\left(f_j\right), & \text{if } \boldsymbol{\mathcal{M}}_{(k,j)} = 1 \\ 0, & \text{if } \boldsymbol{\mathcal{M}}_{(k,j)} = 0, \end{cases} \tag{23}$$

where $0 \leq H_k(f_j) \leq 1$ (avoiding negative amplification values).

An additional constraint is required to guarantee that the number of rings is equal to M. When this constraint is enforced,

$$\mathcal{C}_2 \;:\; \boldsymbol{\mathcal{M}}^T \underline{\mathbf{1}}_{N_{\mathrm{R}} \times 1} = M \cdot \underline{\mathbf{1}}_{N_{\mathrm{R}} \times 1}\,, \tag{24}$$

each column of $\boldsymbol{\mathcal{M}}$ is compelled to include exactly M values different than 0. However, $\mathcal{C}_2$ does not secure that the selected rings between different frequency bins are identically located. A dependency between frequencies can be established by requiring that

$$\mathcal{C}_3 \;:\; \forall j \in [1, J-1] \quad \|\boldsymbol{\mathcal{M}}_j - \boldsymbol{\mathcal{M}}_{j+1}\|_2^2 = 0\,, \tag{25}$$

where $\|\cdot\|_2$ is the ℓ_2-norm and $\boldsymbol{\mathcal{M}}_j$ is the j^{th} column of the binary mask. A correspondence is formed between adjacent frequency bins using constraint $\mathcal{C}_3$. The binary mask must have every adjacent column identical to obtain $\mathcal{C}_3$. So, the optimization problem ensures that rings are consistently selected across the entire frequency range. Note that Constraint (25) is defined in a quadric form to maintain the convexity of the optimization problem.

Next, a constraint to avoid distortion of the signal of interest is introduced. The distortionless response constraint is given by

$$\mathcal{C}_4 \;:\; \forall \{f_j\}_{j=1}^{J} \in \Omega \quad \boldsymbol{\mathcal{H}}_j^T \underline{\boldsymbol{\mathcal{R}}}\left(f_j, \theta_{\mathrm{d}}\right) = 1\,, \tag{26}$$

where $\underline{\boldsymbol{\mathcal{R}}}(f, \theta)$ denotes the ring responses vector, constructed from the response beampattern of each ring in the grid (defined in (13)). The j^{th} column of the weight matrix is denoted by $\boldsymbol{\mathcal{H}}_j$ (meaning the filter applied on the array at frequency f_j). Under constraint $\mathcal{C}_4$, the beampattern is equal to 1 at the direction of arrival.

Additionally, the design of the beamformer aims to maintain a constant beamwidth across a large frequency range. Accordingly, we denote a range of angles of interest by Θ, i.e., the elevation angles enclosed within the main beam $[0, \frac{\theta_{\mathrm{BW}}}{2}] \in \Theta$. We define the concatenated beampattern power vector at an elevation angle θ_i over a set of frequencies as

$$\underline{\boldsymbol{\mathcal{B}}}\left(\theta_i\right) = \begin{bmatrix} \boldsymbol{\mathcal{H}}_1^T \underline{\boldsymbol{\mathcal{R}}}\left(f_1, \theta_i\right) \\ \boldsymbol{\mathcal{H}}_2^T \underline{\boldsymbol{\mathcal{R}}}\left(f_2, \theta_i\right) \\ \vdots \\ \boldsymbol{\mathcal{H}}_J^T \underline{\boldsymbol{\mathcal{R}}}\left(f_J, \theta_i\right) \end{bmatrix}, \tag{27}$$

and denote a set of linear constraints for elevation angles within the mainbeam:

$$\mathcal{C}_5 \;:\; \forall \theta_i \in \Theta \;\; \underline{\boldsymbol{\mathcal{B}}}\left(\theta_i\right) \geq \beta_{\mathrm{BW}} \cdot \underline{\mathbf{1}}_{J \times 1}\,, \tag{28}$$

where β_{BW} marks the -3 dB amplitude. Hence, the beampattern magnitude within the mainbeam should be greater or equal to the magnitude value at the desired beamwidth. It should be noted that the CRA is constructed from a sufficient number of microphones on each ring, as discussed in Section II. As a result, the array is independent of the azimuth angle ϕ. Therefore, we choose an arbitrary ϕ during the optimization process.

B. Directivity Factor Maximization

The constraints presented in Section III-A form a constant beamwidth beamformer with a distortionless response. Under the specified constraints, a set of M rings is chosen from a grid of possible places. As our objective is to maximize the DF under the distortionless response constraint in (26), the cost function can be defined as the sum of all the DF denominators within the frequency range:

$$\min_{\boldsymbol{\mathcal{H}}, \boldsymbol{\mathcal{M}}} \sum_{j=1}^{J} \boldsymbol{\mathcal{H}}_j^T \boldsymbol{\Gamma}\left(f_j\right) \boldsymbol{\mathcal{H}}_j\,. \tag{29}$$

The arguments in the summation are all non-negative. Therefore, the algorithm seeks to determine the optimal constellation of rings to minimize the overall summation result. Note, however, that the optimization is performed not only on the beamformer weights but also on the locations of the rings. In theory, a reduced-degrees-of-freedom optimization may outperform the sparse optimization presented above. If there is a known ring spacing, the optimization can be solved incoherently per frequency bin, resulting in a greater DF in specific frequencies. We suggest a weighted cost function to improve the performance of the nonuniform beamformer. The weighting coefficients would incorporate the results of an incoherent optimization (conducted on a set of uniform rings), as we will demonstrate next.

1) Incoherent Optimization of Uniform CRA: In this section, we consider an optimization problem involving equally-spaced rings. In the uniform scenario, the number of rings and their locations are pre-selected. The solution of the beamformer will be used as a weighting value for the nonuniform beamformer. The uniform beamformer weights are calculated by solving an optimization problem using quadratic programming, defined to optimize the DF in each frequency bin (given determined ring placements). The problem constraints in Section III-A are modified to allow solving each frequency bin independently, as follows: For each frequency, f_j, the distortionless constraint is given by

$$\mathcal{C}_1 \;:\; \underline{\boldsymbol{h}}^T\left(f_j\right) \underline{\boldsymbol{d}}\left(f_j, \theta_{\mathrm{d}}, \phi_{\mathrm{d}}\right) = 1\,. \tag{30}$$

Under this constraint, the DF is maximized by

$$\min_{\underline{\boldsymbol{h}}(f_j)} \quad \underline{\boldsymbol{h}}^T\left(f_j\right) \boldsymbol{\Gamma}\left(f_j\right) \underline{\boldsymbol{h}}^T\left(f_j\right)\,. \tag{31}$$

The desired beamwidth is obtained by requiring

$$\mathcal{C}_2 \;:\; \forall \theta_i \in \Theta \quad \underline{\boldsymbol{h}}^T\left(f_j\right) \underline{\boldsymbol{d}}\left(f_j, \theta_i, \phi\right) \geq \beta_{\mathrm{BW}}\,. \tag{32}$$

Furthermore, to avoid negative amplification values, a third constraint on the weights amplitude is added:

$$\mathcal{C}_3 \;:\; \forall H_m\left(f_j\right) \in \underline{\boldsymbol{h}}\left(f_j\right) \quad 0 \leq H_m\left(f_j\right) \leq 1\,. \tag{33}$$

To sum up, given a frequency f_j the uniform constant beamwidth beamformer weights are calculated by:

$$\begin{aligned}\min_{\underline{\boldsymbol{h}}(f_j)} \quad & \underline{\boldsymbol{h}}^T(f_j)\,\boldsymbol{\Gamma}(f_j)\,\underline{\boldsymbol{h}}^T(f_j) \\ \text{s.t.} \quad & \underline{\boldsymbol{h}}^T(f_j)\,\underline{\boldsymbol{d}}(f_j,\theta_{\mathrm{d}},\phi_{\mathrm{d}}) = 1 \\ & \underline{\boldsymbol{h}}^T(f_j)\,\underline{\boldsymbol{d}}(f_j,\theta_i,\phi) \geq \beta_{\mathrm{BW}} \quad \forall\theta_i \in \Theta \\ & 0 \leq H_m(f_j) \leq 1 \quad \forall H_m(f_j) \in \underline{\boldsymbol{h}}(f_j)\,. \end{aligned} \tag{34}$$

The uniform beamformer is designed by solving (34). Following, the DF of the uniform beamformer is calculated at each frequency according to (16). We define the uniform beamformer DF vector as $\underline{\boldsymbol{\mathcal{D}}}_{\mathrm{u}} = [\mathcal{D}_{\mathrm{u}}(f_1), \mathcal{D}_{\mathrm{u}}(f_2), \ldots, \mathcal{D}_{\mathrm{u}}(f_J)]$, where $\mathcal{D}_{\mathrm{u}}(f_j)$ is the DF value of the uniform beamformer at frequency f_j. Next, the uniform beamformer DF will be incorporated in the nonuniform beamformer to yield superior performance of the nonuniform CRA.

2) Cost Function Modification: To outperform the uniform beamformer, $\underline{\boldsymbol{\mathcal{D}}}_{\mathrm{u}}$ is used as a weighting coefficient for the nonuniform beamformer cost function as:

$$\min_{\boldsymbol{\mathcal{H}},\boldsymbol{\mathcal{M}}} \sum_{j=1}^{J} \mathcal{D}_{\mathrm{u}}(f_j)\,\boldsymbol{\mathcal{H}}_j^T\boldsymbol{\Gamma}(f_j)\,\boldsymbol{\mathcal{H}}_j\,. \tag{35}$$

The weight value in frequency bins in which the uniform beamformer demonstrates a high DF value will be higher. Since the cost function aims to minimize the summation overall, the nonuniform beamformer will be impacted more by high-weighted frequency bins. Therefore, high weighted frequencies would affect the DF denominator and reduce its value. As a result, in frequency bins with higher weight values, the nonuniform beamformer would result in equivalently high DF. Hence, compared to the uniform beamformer, the nonuniform beamformer would produce a similar or better performance.

The sparse constant-beamwidth beamformer can be derived by solving the optimization problem:

$$\begin{aligned}\min_{\boldsymbol{\mathcal{H}},\boldsymbol{\mathcal{M}}} \quad & \sum_{j=1}^{J} \mathcal{D}_{\mathrm{u}}(f_j)\,\boldsymbol{\mathcal{H}}_j^T\boldsymbol{\Gamma}(f_j)\,\boldsymbol{\mathcal{H}}_j \\ \text{s.t.} \quad & \mathbf{0} \leq \boldsymbol{\mathcal{H}} \leq \boldsymbol{\mathcal{M}} \\ & \boldsymbol{\mathcal{M}}^T\underline{\mathbf{1}}_{N_{\mathrm{R}}\times 1} = M\cdot\underline{\mathbf{1}}_{N_{\mathrm{R}}\times 1} \\ & \|\boldsymbol{\mathcal{M}}_j - \boldsymbol{\mathcal{M}}_{j+1}\|_2^2 = 0 \quad \forall j \in [1, J-1] \\ & \boldsymbol{\mathcal{H}}_j^T\underline{\boldsymbol{\mathcal{R}}}(f_j,\theta_{\mathrm{d}}) = 1 \quad \forall\{f_j\}_{j=1}^{J} \in \Omega \\ & \underline{\boldsymbol{\mathcal{B}}}(\theta_i) \geq \beta_{\mathrm{BW}}\cdot\underline{\mathbf{1}}_{J\times 1} \quad \forall\theta_i \in \Theta\,. \end{aligned} \tag{36}$$

C. Time Domain Filter Implementation

In a physical setup, the beamformer filters are implemented through temporal finite impulse response (FIR) filters. In the previous section, the weight matrix described the ideal beamformer given the problem constraints. In this section, we approximate the ideal beamformer by using FIR filters implemented in the time domain.

To achieve an accurate beamformer response with a sufficient number of filter taps, the ideal filters should be continuous. Therefore, an additional pre-processing step is added to the beamformer design: After solving (36), we examine the resulting weight matrix. For each ring (chosen by the optimized solution), an effective frequency band is determined. That is, we determine the frequency range in which each ring participates in the beamforming process (attenuated with a weight value above 0). In the following step, the incoherent optimization as in (34) is repeated. However, this time the optimization is performed on the set of non-uniformly spaced rings that participate in each frequency. This step yields an improved weights matrix, with smoothed filters per ring.

The suggested pre-processing step has two significant advantages. First, the desired filters responses are modified to continuous forms. A smooth frequency response requires fewer FIR coefficients to achieve an approximate response of the ideal characteristics. Thus, in the perspective of a physical setup, the designed beamformer requires fewer resources and maintenance and is lower in cost. Second, having a restricting effective frequency range for each ring enables the use of fewer microphones per ring. Note that in (15), the number of microphone elements on each ring is determined by the maximal frequency in which the ring is effective. Without the bandwidth limitation, for each ring we get $\forall m \in [1, M]\ \ f_m^{\max} = 8$ kHz. By adding the frequency restriction, some rings will have a lower value of $f_m^{\max}$, meaning that fewer microphones are required in the CRA.

Following the weight matrix modification, the FIR filters were designed for each ring using the MATLAB Signal Processing toolbox. The design process minimizes the integrated square error between the actual filter response and the ideal filter response [51]

$$\epsilon = \int_0^{\pi} \left(\hat{H}(\omega) - H(\omega)\right)^2 d\omega\,, \tag{37}$$

where ω is the normalized frequency, $\hat{H}(\omega)$ is the actual filter response and $H(\omega)$ is the ideal response. To maintain a fixed time delay, all the FIR filters were designed to have 32 coefficients each. The design process of the nonuniform constant beamwidth beamformer is summarised in Algorithm 1.

IV. Experimental Results

In this section, we compare the uniform beamformer (U-CRA) and the nonuniform beamformer (NU-CRA), both designed to attain constant elevation beamwidth while maximizing the DF. The results shown in this section are for CRA beamformers designed to attain the beamwidth of $\theta_{\mathrm{BW}} = 30^{\circ}$. The beamwidth is defined at the -3 dB amplitude, marked as β_{BW}. The number of the microphone elements in each ring is set according to (15) to prevent spatial aliasing. Note that for both beamformers, the bandwidth limitation for each ring was applied. As described in Section III-C, following the initial optimization, a pre-processing step was added, restricting each ring to be effective at specified frequency bands. The optimization problems shown in (34) and (36) were solved using the MATLAB CVX toolbox [52]. The solver used in these problems is the MOSEK solver, which is a third-party software package. The MOSEK software is extensively used to solve sparse large-scale problems, specifically quadric form optimization.

Algorithm 1: Nonuniform Constant Beamwidth CRA.

Initialization: set the desired number of rings in the array M, the discretized frequency space Ω and the elevation angle range Θ.
Weighting Coefficients Calculation:
define a uniformly spaced CRA with M rings.
for $f = f_j \quad \forall f_j \in \Omega$ **do**
  solve (34).
  update $\underline{\boldsymbol{\mathcal{D}}}_{\mathrm{u}}$ at f_j.
end for
Design the Sparse Nonuniform Beamformer:
define the radii grid $\underline{\boldsymbol{r}}$.
solve (36).
Smooth the Weight Matrix:
for $f = f_j \quad \forall f_j \in \Omega$ **do**
  define the effective rings in the CRA.
  solve (34) on the nonuniform geometry.
end for
Implement the Desired Filters in Time Domain.

In terms of computational complexity, the joint weights constraint has a significant impact on the optimization convergence and runtime. Since the number of parameters in the problem is determined by the number of rings rather than the number of sensors in the array, the problem is simplified, and the optimization converges. Next, the filters were implemented in the time domain and applied to the CRAs. It should be mentioned that the computation time of the U-CRA beamformer is lower than the NU-CRA beamformer (depending on the grid size). However, the NU-CRA beamformer results in better performance measures, as will be presented next.

A. Number of Rings Selection

The user-selected parameters in the design process are the desired beamwidth and the number of rings in the CRA. Selecting the number of rings has a major impact on the beamformer performance. The number of rings affects the robustness of the array, the beampattern characteristics, and the required physical hardware. Thus, while aiming to achieve optimal performance under minimal cost, the user should mitigate the tradeoff by selecting the appropriate number of rings. In addition, the desired beamwidth also influences the array's competence in achieving the specified beamwidth. Hence, selecting fewer rings can result in degradation of the beamwidth in higher frequencies.

The dependency on the number of selected rings in the CRA is shown in Fig. 3, plotting the DF and WNG of the U-CRA beamformer for different numbers of rings. As expected, as the number of rings in the CRA increases, the DF and WNG are improved. However, note that starting from a certain number of rings (8 in the presented setup), there is a minor improvement when adding more rings. Hence, there is a point from which adding more rings is redundant. The saturation point depends on the desired beamwidth and the maximal diameter of the CRA.

For a smaller number of rings (4 and 6), the DF decreases at high frequencies. Since the rings are equally spaced, choosing

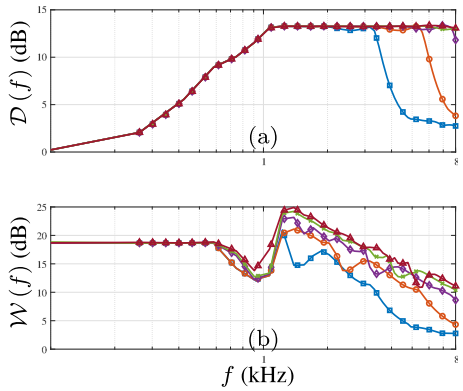

Fig. 3. Performance measures of the U-CRA beamformer with 4 rings (square), 6 rings (circle), 8 rings (diamond), 10 rings (cross), and 12 rings (triangle). (a) DF and (b) WNG, as a function of frequency.

fewer rings results in farther ring placements. At high frequencies, the inner-most ring and the adjacent ring are the dominant rings in the beamforming process. As a result, the beampattern characteristics are set according to the smaller ring radii. By examining the beampattern of a continuous ring, we note that as the ring radius is bigger, the mainlobe is narrower, and the sidelobes are higher. Consequently, the sparse U-CRA incorporates wider rings in the beamforming process at high frequencies to attain the specified beamwidth, leading to a decrease in the DF. A detailed analysis of the beampattern features concerning the radius and frequency is provided in [45]. In the following sections, the advantages of the NU-CRA for a small number of rings are presented. In the nonuniform configuration, the resulting CRA incorporates smaller radii rings in high frequencies and larger rings in low frequencies. Thus, the performance of the NU-CRA is superior compared to the U-CRA with an equal number of rings.

B. Nonuniform Beamformer Simulation Results

The NU-CRA beamformer weights were calculated for a grid containing $N_{\mathrm{R}} = 100$ equally spaced rings in the radii range $\underline{\boldsymbol{r}} \in [0, 25]$ cm. Note that the initial grid size affects the number of parameters in the optimization problem. Thus, initializing a finer grid may result in better ring constellations, but will lead to longer convergence times. Storage limitations should also be considered before grid initialization to avoid memory errors while solving the optimization problem. As the number of desired rings in the CRA increases, the grid should include more possible radii.

A set of $M = 5$ rings where selected from the problem solution at radii $\underline{\boldsymbol{r}}_{\mathrm{opt}} = [2, 4.8, 8.1, 13.9, 25]$ cm, with approximately logarithmic scaling of 2, as shown in Fig. 4(a).

The resulting ring spacing is not linear, and the spacing between two adjacent rings gradually grows from the inner ring to the outer one. Fig. 4(b) shows the beamformer weights. The y-axis represents frequency bins used for designing the array filters, and the x-axis represents the ring index (1–5), where index 1 is the inner-most ring. In the lower frequency range, the optimized solution includes the outer-most ring solely. This selection is preferred for DF as the beamwidth of the outer ring is narrower

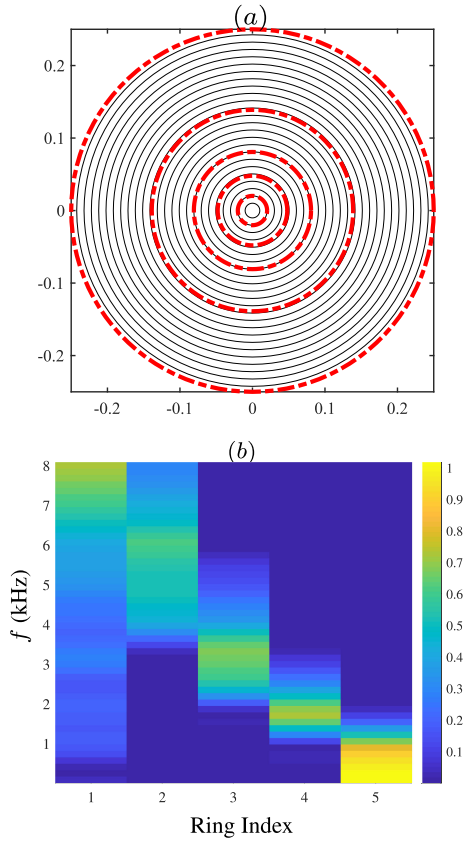

Fig. 4. Constant beamwidth optimized NU-CRA beamformer. (a) Chosen rings (dashed-red) out of the optional radii grid. The grid was downsampled for visualization reasons. (b) Beamformer weight values applied to the array at each frequency.

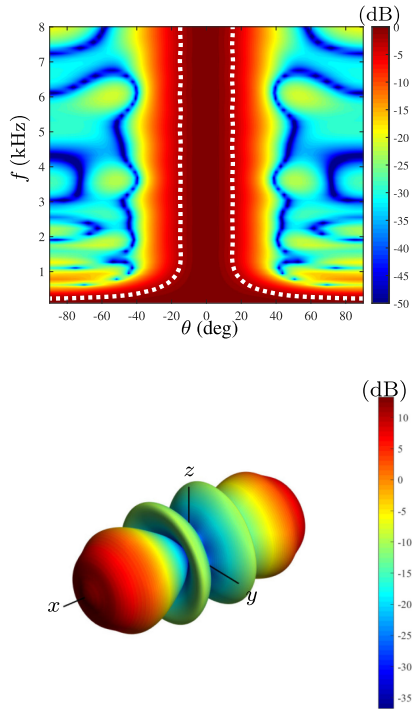

Fig. 5. (top) Beampattern of a 5-ring CRA, attenuated with the nonuniform beamformer filters. The dashed line marks the main lobe's half-power (-3 dB) points. (Bottom) 3D Beampattern of a 5-ring CRA nonuniform beamformer at $f = 5.6$ kHz.

in low frequencies than the remainder of the CRA rings. The relation between the ring radius and the beamwidth is evident from the properties of the zero-order Bessel function [49]. As the frequency increases, the beamforming is done by weighting the inner-most ring and one of the outer rings, gradually decreasing the outer rings' weight and minimizing the effective radius. Hence, by controlling the beampattern tradeoff between the inner ring and a single ring beampattern with decreasing radius - the beamwidth is kept constant. In addition, the frequency responses of the FIR filters produced per ring are continuous and do not contain any irregularities.

The beampattern amplitude is shown in Fig. 5(a), with dashed lines highlighting the main lobe's half-power (-3 dB) points. The beamwidth is maintained constant in the specified θ_{BW} over a range of frequencies $f \in [1, 8]$ kHz. Hence, the suggested constraints in problem (36) ensure a frequency-invariant beamwidth in the attainable frequency range. In addition, we note that the sidelobe level is low compared to the mainbeam (which is desired when the beamformer aims to maximize the DF).

Fig. 5(b) presents the 3D beampattern at $f = 5.6$ kHz. Due to the circular symmetry, the beampattern remains constant as the azimuth angle varies. In addition, we note that since the mainlobe is directed to the broadside at $\theta = 0^\circ$, the performance of the beamformer with the joint weights constraints is similar to a beamformer without the constraint. As mentioned in Section II, the proposed system eliminates beam-steering and focuses on constant elevation beamwidth. Without steering, the result of a beamformer with individual microphone weights would be similar to the presented beamformer. However, the joint weights enable to reduce the hardware complexity and improve the stability and convergence of real-time beamwidth control implementations.

C. Performance Measures Comparison

As mentioned in Section II, the DF and WNG are important characteristics of any beamformer. The main objective of the suggested beamformers was to gain maximal DF while maintaining fixed beamwidth. Thus, the DF as a function of frequency is presented in Fig. 6(a). While both beamformers attain constant beamwidth, compared to the U-CRA beamformer (dashed-triangle plot), the NU-CRA design (pointed-square plot) shows superior performance in frequencies where $4\text{ kHz} < f$. The maximal difference between the beamformers is $\approx$10 dB in the DF. Due to the optimized selection of ring positions in the NU-CRA beamformer, the beampattern characteristics are preferred in terms of DF. In addition, a comparison between the proposed NU-CRA and the NU-CRA without the cost function weighting demonstrates the advantages of the suggested modification. Adding the uniform DF as weighting coefficients in the NU-CRA cost function results in a 3 dB improvement of the DF in the frequency range $f \in [1.6, 3.4]$ kHz. Moreover, the WNG is approximately equal between the two approaches.

Fig. 6(b) plots the WNG of the discussed beamformers. Note that in lower frequencies having $f <$ 0.6 kHz, the WNG of the NU-CRA is 1 dB higher compared to the U-CRA. In the lower

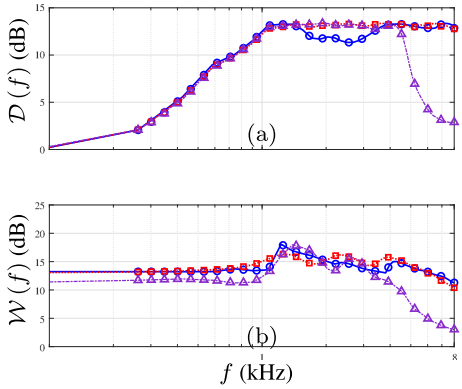

Fig. 6. Performance measures for 5-ring U-CRA (dash-dot line with triangles), NU-CRA (dotted line with squares), and the NU-CRA without the cost function weights (solid-circle line) beamformers. (a) DF and (b) WNG, as a function of frequency. The x-axis is log-scaled for presentation.

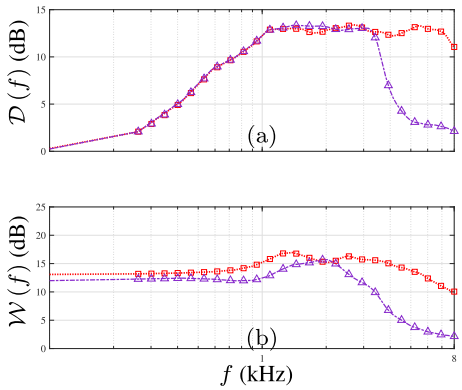

Fig. 7. Performance measures for 4-ring U-CRA (dash-dot line with triangles) and NU-CRA (dotted line with squares) beamformers. (a) DF and (b) WNG, as a function of frequency.

frequency range, both beamformers include the outer-most ring solely. Since the outer ring in the NU-CRA is effective in higher frequencies compared to the U-CRA, it includes more microphone elements. As a result, the WNG of the NU-CRA in that frequency range is a bit higher. In higher frequencies, the NU-CRA presents higher WNG, with an average difference of 7 dB. The decrease of the WNG of the U-CRA beamformer at these frequencies is caused due to a high weight value given to the central microphone (a single microphone at the center of the CRA). In the U-CRA beamformer the rings are equally spaced in the range $\underline{r} \in [0, 25]$ cm, meaning that the inner-most ring is a single microphone in the center of the array. The NU-CRA beamformer solution yielded the inner-most ring in $r = 2$ cm, constructed of 6 equally spaced microphones. As a result, the U-CRA depends on the central microphone, affecting the robustness of the array to microphone imperfections, which is reflected by the WNG.

To examine the dependency on the number of rings in the array, Fig. 7 presents the performance measures of the U-CRA and NU-CRA beamformers constructed of 4 rings (compared to the 5 rings array shown in Fig. 6). First, we note that the enhanced performance in terms of DF and WNG of the NU-CRA is consistent in the 4 ring constellation. Second, comparing Figs. 6(a) and 7(a) demonstrates an additional advantage of the

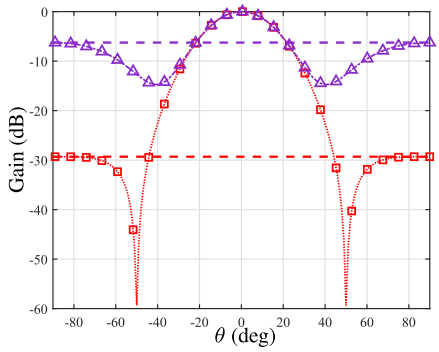

Fig. 8. Beampattern for $f = 5000$ Hz calculated for U-CRA (dash-dot line with triangles) and NU-CRA (dotted line with squares) beamformers. The first sidelobe level of each beampattern is marked by a dashed line.

NU-CRA beamformer: given a smaller number of rings, the improvement of the DF is established in lower frequencies. In Fig. 7(a), the NU-CRA DF is higher than the U-CRA starting from 3.1 kHz $< f$. In the 5 rings array, the improvement of the DF is noted from 4 kHz $< f$. Hence, when the number of rings is smaller, the frequency range in which the NU-CRA outperforms the U-CRA is wider, making the NU-CRA a preferable choice.

Out-of-beamwidth signals can interrupt and distort the output signal. The sidelobe attenuation can be helpful in the suppression of the noise signals and enhance the DF. Fig. 8 shows the beampattern of the discussed beamformers at frequency $f = 5$ kHz. The frequency was chosen out of the frequency range in which the desired beamwidth is attained. There is a significant 24 dB difference in the first sidelobe level between the beamformers. The gap between the sidelobe levels is reflected in the DF comparison as discussed above. Additional frequencies in the range demonstrated corresponding relations between the sidelobe levels.

V. Conclusion

We have presented broadband beamforming methods for concentric circular arrays, which are broadly used in audio communication applications. The objective of the presented beamformers is to control the elevation beamwidth while optimizing the DF across a wide range of frequencies. The designs assume different degrees of freedom in the array geometry and the beamformer constraints. A constant beamwidth beamformer aiming to optimize the DF on a set of given ring radii was suggested. The incoherent optimization problem, was solved for each frequency bin separately, and the constraints enabling a constant beamwidth were presented and applied on an equally spaced CRA. In addition, a coherent beamformer was proposed to sparsely select the optimal rings placements while simultaneously achieving the problem specifications. To ensure a joint selection of rings over the entire frequency range, a new set of constraints was presented employing the properties of a binary mask. Furthermore, to ensure the equal or higher performance of the sparse beamformer, the incoherent beamformer was utilized as a weighting coefficient in the coherent cost function.

The sparse optimization yielded a non-uniformly spaced CRA. Simulations show that the proposed coherent and incoherent beamforming methods attained comparable high

directivity, yet the nonuniform beamformer outperforms the uniform beamformer. The advantages of the nonuniform beamformer were also shown for a different CRA configuration, constructed of fewer rings. Hence, based on the design restrictions, one can apply the suggested methodology to attain superior performance concerning the DF. The proposed beamformers apply the same filter to all the elements on each ring, resulting in reduced computational complexity in the design process and fewer resources in a physical setup. The computational complexity is a crucial factor in the convergence of the optimized solution. In addition, a limitation to the effective beamwidth of each ring in the CRA was suggested. The beamwidth limitation enabled the use of fewer microphones per ring while attaining the desired beampattern properties. A time-domain implementation of the ideal beamformer filters was presented and applied to the CRAs. Future research may focus on additional parameter optimizations, diverse array geometries, and numerical algorithms to solve the optimization problem in real time.

ACKNOWLEDGMENT

The authors would like to thank Stem Audio for providing equipment and technical guidance.

REFERENCES

[1] M. Brandstein and D. Ward, Eds., *Microphone Arrays: Signal Processing Techniques and Applications* (Digital signal processing Series). New York, NY, USA: Springer, 2001.

[2] B. V. Veen and K. Buckley, "Beamforming: A versatile approach to spatial filtering," *IEEE ASSP Mag.*, vol. 5, no. 2, pp. 4–24, Apr. 1988.

[3] C. A. Balanis, *Antenna Theory: Analysis and Design*. Hoboken, NJ,USA: Wiley, 2016.

[4] D. B. Ward, R. A. Kennedy, and R. C. Williamson, "Theory and design of broadband sensor arrays with frequency invariant far–field beam patterns," *J. Acoust. Soc. Amer.*, vol. 97, pp. 1023–1034, Feb. 1995.

[5] T. Chou, "Frequency-independent beamformer with low response error," in *Proc. IEEE Int. Conf. Acoust., Speech, Signal Process.*, Detroit, MI, USA, 1995, vol. 5, pp. 2995–2998.

[6] S. Gannot, D. Burshtein, and E. Weinstein, "Signal enhancement using beamforming and nonstationarity with applications to speech," *IEEE Trans. Signal Process.*, vol. 49, no. 8, pp. 1614–1626, Aug. 2001.

[7] W. Liu and S. Weiss, "New class of broadband arrays with frequency invariant beam patterns," in *Proc. IEEE Int. Conf. Acoust., Speech, Signal Process.*, Montreal, QC, Canada, 2004, vol. 2, pp. ii-185–8.

[8] S. Markovich, S. Gannot, and I. Cohen, "Multichannel eigenspace beamforming in a reverberant noisy environment with multiple interfering speech signals," *IEEE Trans. Audio, Speech, Lang. Process.*, vol. 17, no. 6, pp. 1071–1086, Aug. 2009.

[9] W. Liu, "Adaptive wideband beamforming with sensor delay-lines," *Signal Process.*, vol. 89, pp. 876–882, May 2009.

[10] M. Crocco and A. Trucco, "Design of robust superdirective arrays with a tunable tradeoff between directivity and frequency-invariance," *IEEE Trans. Signal Process.*, vol. 59, no. 5, pp. 2169–2181, May 2011.

[11] Y. Zhao and W. Liu, "Robust fixed frequency invariant beamformer design subject to norm-bounded errors," *IEEE Signal Process. Lett.*, vol. 20, no. 2, pp. 169–172, Feb. 2013.

[12] R. Berkun, I. Cohen, and J. Benesty, "Combined beamformers for robust broadband regularized superdirective beamforming," *IEEE/ACM Trans. Audio, Speech, Lang. Process.*, vol. 23, no. 5, pp. 877–886, May 2015.

[13] J. Benesty, I. Cohen, and J. Chen, *Fundamentals of Signal Enhancement and Array Signal Processing*. Hoboken, NJ, USA: Wiley, 2018.

[14] W. P. M. N. Keizer, "Fast low-sidelobe synthesis for large planar array antennas utilizing successive fast Fourier transforms of the array factor," *IEEE Trans. Antennas Propag.*, vol. 55, no. 3, pp. 715–722, Mar. 2007.

[15] L. Manica, P. Rocca, and A. Massa, "Design of subarrayed linear and planar array antennas with SLL control based on an excitation matching approach," *IEEE Trans. Antennas Propag.*, vol. 57, no. 6, pp. 1684–1691, Jun. 2009.

[16] J. Wu, W. N. Huang, Y. J. Cheng, and Y. Fan, "A broadband high-gain planar array antenna for V-band wireless communication," in *Proc. IEEE 3rd Asia-Pacific Conf. Antennas Propag.*, Harbin, China, 2014, pp. 309–312.

[17] G. Huang, J. Chen, and J. Benesty, "On the design of differential beamformers with arbitrary planar microphone array geometry," *J. Acoust. Soc. Amer.*, vol. 144, pp. E L66–EL70, Jul. 2018.

[18] C. Mathews and M. Zoltowski, "Eigenstructure techniques for 2-D angle estimation with uniform circular arrays," *IEEE Trans. Signal Process.*, vol. 42, no. 9, pp. 2395–2407, Sep. 1994.

[19] P. Ioannides and C. Balanis, "Uniform circular arrays for smart antennas," *IEEE Antennas Propag. Mag.*, vol. 47, no. 4, pp. 192–206, Aug. 2005.

[20] E. Tiana-Roig, F. Jacobsen, and E. F. Grande, "Beamforming with a circular microphone array for localization of environmental noise sources," *J. Acoust. Soc. Amer.*, vol. 128, pp. 3535–3542, 2010.

[21] A. M. Torres, M. Cobos, B. Pueo, and J. J. Lopez, "Robust acoustic source localization based on modal beamforming and time-frequency processing using circular microphone arrays," *J. Acoust. Soc. Amer.*, vol. 132, pp. 1511–1520, Sep. 2012.

[22] S. Yan, "Optimal design of modal beamformers for circular arrays," *J. Acoust. Soc. Amer.*, vol. 138, pp. 2140–2151, Oct. 2015.

[23] Y. Li, K. Ho, and C. Kwan, "Beampattern synthesis for concentric circular ring array using MMSE design," in *Proc. IEEE Int. Symp. Circuits Syst.*, vol. 3, 2004, pp. III–329.

[24] L. Zhao, J. Benesty, and J. Chen, "Design of robust differential microphone arrays with the Jacobi-Anger expansion," *Appl. Acoust.*, vol. 110, pp. 194–206, Sep. 2016.

[25] Y. Wang and Y. Yang, "A flexible method for designing frequency-invariant beamformers with circular sensor arrays," *IEEE Access*, vol. 6, pp. 57 073–57 084, 2018.

[26] S. C. Chan and H. H. Chen, "Uniform concentric circular arrays with frequency-invariant characteristics–Theory, design, adaptive beamforming and DOA estimation," *IEEE Trans. Signal Process.*, vol. 55, no. 1, pp. 165–177, Jan. 2007.

[27] H. H. Chen, S. C. Chan, Z. G. Zhang, and K. L. Ho, "Adaptive beamforming and recursive DOA estimation using frequency-invariant uniform concentric spherical arrays," *IEEE Trans. Circuits Syst. I: Regular Papers*, vol. 55, no. 10, pp. 3077–3089, Nov. 2008.

[28] Y. Zhao, W. Liu, and R. Langley, "Application of the least squares approach to fixed beamformer design with frequency-invariant constraints," *IET Signal Process.*, vol. 5, pp. 281–291, 2011.

[29] X. Zhao, Q. Yang, and Y. Zhang, "A hybrid method for the optimal synthesis of 3-D patterns of sparse concentric ring arrays," *IEEE Trans. Antennas Propag.*, vol. 64, no. 2, pp. 515–524, Feb. 2016.

[30] Y. Buchris, A. Amar, J. Benesty, and I. Cohen, "Incoherent synthesis of sparse arrays for frequency-invariant beamforming," *IEEE/ACM Trans. Audio, Speech, Lang. Process.*, vol. 27, no. 3, pp. 482–495, Mar. 2019.

[31] Y. Buchris, I. Cohen, J. Benesty, and A. Amar, "Joint sparse concentric array design for frequency and rotationally invariant beampattern," *IEEE/ACM Trans. Audio, Speech, Lang. Process.*, vol. 28, pp. 1143–1158, 2020.

[32] J. Benesty, J. Chen, and I. Cohen, *Design of Circular Differential Microphone Arrays* (Springer Topics in Signal Processing Series), vol. 12. Cham, Switzerland: Springer, 2015.

[33] Y. Buchris, I. Cohen, and J. Benesty, "Asymmetric beampatterns with circular differential microphone arrays," in *Proc. IEEE Workshop Appl. Signal Process. Audio Acoust.*, 2017, pp. 190–194.

[34] G. Huang, J. Benesty, and J. Chen, "Design of robust concentric circular differential microphone arrays," *J. Acoust. Soc. Amer.*, vol. 141, pp. 3236–3249, May 2017.

[35] Y. Yang, C. Sun, and C. Wan, "Theoretical and experimental studies on broadband constant beamwidth beamforming for circular arrays," in *Proc. Oceans. Celebrating Past... Teaming Toward Future*, 2003, vol. 3, pp. 1647–1653.

[36] X. Zhang, W. Ser, and K. Muralidhar, "Uniform circular broadband beamformer with selective frequency and spatial invariant region," in *Proc. IEEE Int. Symp. Circuits Syst.*, 2009, pp. 2201–2204.

[37] X. Zhang, W. Ser, Z. Zhang, and A. Krishna, "Selective frequency invariant uniform circular broadband beamformer," *EURASIP J. Adv. Signal Process.*, vol. 2010, Dec. 2010, Art. no. 678306.

[38] F. Borra, A. Bernardini, F. Antonacci, and A. Sarti, "Efficient implementations of first-order steerable differential microphone arrays with arbitrary planar geometry," *IEEE/ACM Trans. Audio, Speech, Lang. Process.*, vol. 28, pp. 1755–1766, 2020, doi: 10.1109/TASLP.2020.2998283.

[39] J. Wang, Q. Feng, R. Wu, and Z. Su, "A constant-beamwidth beamforming method for acoustic imaging," in *Proc. IEEE Antennas Propag. Soc. Int. Symp.*, Honolulu, HI, 2007, pp. 4236–4239.

[40] S. Li, X. Yang, L. Ning, T. Long, and T. K. Sarkar, "Broadband constant beamwidth beamforming for suppressing mainlobe and sidelobe interferences," in *Proc. IEEE Radar Conf.*, Seattle, WA, USA, 2017, pp. 1041–1045.
[41] O. Rosen, I. Cohen, and D. Malah, "FIR-based symmetrical acoustic beamformer with a constant beamwidth," *Signal Process.*, vol. 130, pp. 365–376, Jan. 2017.
[42] T. Long, I. Cohen, B. Berdugo, Y. Yang, and J. Chen, "Window-based constant beamwidth beamformer," *Sensors*, vol. 19, May 2019, Art. no. 2091.
[43] R. Sharma, I. Cohen, and B. Berdugo, "Controlling elevation and azimuth beamwidths with concentric circular microphone arrays," *IEEE/ACM Trans. Audio, Speech, Lang. Process.*, vol. 29, pp. 1491–1502, 2021, doi: 10.1109/TASLP.2021.3072275.
[44] R. Sharma, I. Cohen, and B. Berdugo, "Window beamformer for sparse concentric circular array," in *Proc. IEEE Int. Conf. Acoust., Speech Signal Process.*, 2021, pp. 4500–4504.
[45] A. Kleiman, I. Cohen, and B. Berdugo, "Constant-beamwidth beamforming with concentric ring arrays," *Sensors*, vol. 21, pp. 7253–7271, Nov. 2021.
[46] A. Beck, *Introduction to Nonlinear Optimization: Theory, Algorithms, and Applications With MATLAB (MOS-SIAM Series on Optimization)*. Philadelphia,PA, USA: Soc. Ind. Appl. Math., 2014.
[47] Y. Li, K. C. Ho, and C. Kwan, "3-D array pattern synthesis with frequency invariant property for concentric ring array," *IEEE Trans. Signal Process.*, vol. 54, no. 2, pp. 780–784, Feb. 2006.
[48] R. L. Haupt, "Optimized element spacing for low sidelobe concentric ring arrays," *IEEE Trans. Antennas Propag.*, vol. 56, no. 1, pp. 266–268, Jan. 2008.
[49] C. T. Molloy, "Calculation of the directivity index for various types of radiators," *J. Acoust. Soc. Amer.*, vol. 20, pp. 387–405, Jul. 1948.
[50] R. A. Mucci and R. G. Pridham, "Comparison of shifted sideband and conventional beamforming techniques," *J. Acoust. Soc. Amer.*, vol. 65, pp. S61–S61, Jun. 1979.
[51] A. V. Oppenheim, R. W. Schafer, and J. R. Buck, *Discrete-Time Signal Processing*. Upper Saddle River, NJ, USA: Prentice Hall, 1999.
[52] M. Grant and S. Boyd, "CVX: Matlab software for disciplined convex programming," version 2.1, Mar. 2014. [Online]. Available: http://cvxr.com/cvx

Avital Kleiman received the B.Sc. degree in electrical engineering and physics and the M.Sc. degree in electrical engineering from the Technion–Israel Institute of Technology, Haifa, Israel, in 2016 and 2022, respectively. Her research interests include array processing and microphone arrays.

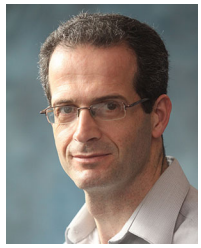

Israel Cohen (Fellow, IEEE) received the B.Sc. (*Summa Cum Laude*), M.Sc., and Ph.D. degrees in electrical engineering from the Technion – Israel Institute of Technology, Haifa, Israel, in 1990, 1993, and 1998, respectively. He is currently the Louis and Samuel Seidan Professor of electrical and computer engineering with the Technion – Israel Institute of Technology.

From 1990 to 1998, he was a Research Scientist with RAFAEL Research Laboratories, Haifa, Israel Ministry of Defense. From 1998 to 2001, he was a Postdoctoral Research Associate with the Computer Science Department, Yale University, New Haven, CT, USA. In 2001, he joined the Electrical Engineering Department of the Technion. He is a coeditor of the Multichannel Speech Processing Section of the *Springer Handbook of Speech Processing* (Springer, 2008) and the coauthor of *Fundamentals of Signal Enhancement and Array Signal Processing* (Wiley-IEEE Press, 2018). His research interests include array processing, statistical signal processing, deep learning, analysis and modeling of acoustic signals, speech enhancement, noise estimation, microphone arrays, source localization, blind source separation, system identification, and adaptive filtering.

Dr. Cohen was the recipient of the Norman Seiden Prize for Academic Excellence (2017), SPS Signal Processing Letters Best Paper Award (2014), Alexander Goldberg Prize for Excellence in Research (2010), and Muriel and David Jacknow Award for Excellence in Teaching (2009). He was as an Associate Editor for the IEEE TRANSACTIONS ON AUDIO, SPEECH, AND LANGUAGE PROCESSING and IEEE SIGNAL PROCESSING LETTERS, a Member of the IEEE Audio and Acoustic Signal Processing Technical Committee and IEEE Speech and Language Processing Technical Committee, and a Distinguished Lecturer of the IEEE Signal Processing Society.

Baruch Berdugo received the B.Sc. (Cum Laude) and M.Sc. degrees in electrical engineering, and the Ph.D. degree in biomedical engineering from the Technion - Israel Institute of Technology, Haifa, Israel, in 1978, 1987, and 2001, respectively. He is currently a Research Associate in electrical engineering with the Technion - Israel Institute of Technology. From 1982 to 2001, he was a Research Scientist with RAFAEL Research Laboratories, Haifa, Israel Ministry of Defense. From 2001 to 2003, he was the General Manger of Lamar Signal Processing, Yoqneam Ilit, Israel. From 2004 to 2018, he was the General Manager of MRD technologies, Kibbutz Usha, Israel, and the CTO of Phoenix Audio Technologies, Irvine CA USA. His research interests include array processing, statistical signal processing, deep learning, analysis, speech enhancement, noise estimation, microphone arrays, source localization, and adaptive filtering.